NUMERICAL INVESTIGATION OF THE EFFECT OF INFLOW DISTORTIONS ON TRANSONIC AXIAL COMPRESSOR STAGES WITH 2D AND 3D CALCULATIONS

Andreas Lesser, Sebastian Barthmes, Reinhard Niehuis
Institut for Jet Propulsion,
Universität der Bundeswehr München
andreas.lesser@unibw.de, sebastian.barthmes@unibw.de, reinhard.niehuis@unibw.de

Keywords: *axial transonic compressor, inflow distortion, numerical simulation*

Abstract

Non-uniform compressor inflow is a common problem, not only when operating jet engines but also with industrial gas turbines. Some recent developments of modern high efficient airframe concepts e.g. consider installation of boundary layer ingesting engines, i.e. engines which are permanently impinged on by inhomogeneous inflow conditions. Therefore, the behavior of the engine's compressor towards distorted inflow has to be taken into account already early in the design phase. The influence of distorted inflow on two different compressor stages is investigated in this paper by full-annulus 3D as well as by 2D blade-to-blade calculations. Unsteady full-annulus 3D computations of the whole compressor system are still very time-consuming. Hence, this paper investigates and validates the potential of 2D full-annulus blade-to-blade simulation. In how far the flow field can be validly predicted by 2D blade-to-blade simulations depends strongly on the radial deviation of the stream-tubes and on secondary flow effects. For this reason, this study includes two different transonic axial compressors. The first one has a high aspect ratio and a small tip clearance gap resulting in a weak tip clearance vortex and secondary flow influence. In contrast to this first one, the second compressor was designed for a 3D dominated passage flow with a small aspect ratio and a large tip clearance gap. Both compressors were simulated in 2D as well as in full 3D, with a total pressure distortion that was steady, constant in radial, but varying in circumferential direction. The objective of this study is to investigate the influence of a total pressure distortion on two different compressor stages in terms of flow field deviation and mechanical blade loading as well as to access the quality of the predicted flow-field of 2D bade-to-blade calculations, compared to full 3D calculations.

Nomenclature

p	Pressure
T	Temperature
α	Inflow angle

Subscripts

0	Inlet condition
1	Rotor inlet plane
2	Plane between rotor and stator

1 Introduction

High efficiency is a crucial feature for modern gas turbine engines. The effect of distorted inflow on the performance of turbomachines is relevant, both for industrial gas turbines and for jet engines. Distorted inflow can result from various flow phenomena, such as ground vortices, inlet flow separation at high angles of attack, or wakes of inlet struts. These distortions influence the stall margin as well as the compressor's performance and efficiency, and therefore of the efficiency of the whole engine. A general overview of the effect of inlet distortions is given in [1]. In the last years, the

influence on the efficiency has become more important [2], [3,4], in contrast to earlier investigations, such as [5], which focused on the stability of the compressor. On the one hand, this is due to the economic demand for high efficient engines, on the other hand, future airframe designs will include boundary layer ingesting engines, i.e. they will have to deal with permanent distorted compressor inflow. Therefore, the process of designing a modern jet engine will be increasingly concerned with the influence of such distortions. The numerical prediction of flow features already plays an important role in the aerodynamic design process. However, three dimensional, full-annulus simulations of the compressor with distorted inflow are still computational very expensive, although they would be required for the correct numerical simulation of all occurring flow features. An attractive alternative are 2D, full-annulus, blade-to-blade simulations. However, 2D simulations lead to a loss of prediction quality, mainly due to the 3D flow character and due to secondary flow effects. Both 3D flow character and secondary flows are inherent characteristics of each compressor and depend on design features, such as aspect-ratio, blade design, and clearances. Hence in this study, 2D as well as 3D full-annulus calculations are carried out for two transonic compressors, with different design philosophies and therefore distinct differences in terms of the 3D flow field.

2 Compressor Test Cases

The first part of the engine interacting with distorted inflow is the fan stage, which is transonic in modern jet engines. Hence both compressor stages under consideration here are transonic and axial. Other common design features are a radial constant energy addition along the blade height, and an axial inlet and outlet flow.

2.1. DLR compressor stage

The first compressor stage investigated in this study is a transonic high-pressure compressor, operated at the DLR institute of propulsion technology (Dunker [6,7] and Lecht [5]). The experimental setup can be seen in Figure 1. The rotor is designed with double-circular-arc-blades (DCA) for the subsonic part near hub, and with multiple-circular-arc-blades (MCA) for the supersonic part near tip where the maximum relative inflow Mach number 1.4 is reached. Overall, the rotor consists of 28 blades with an average chord length of 50 mm. The stator consists of 72 vanes with NACA-65 profiles. In this configuration, detailed measurements of temperature, pressure, and flow angle exist only under disturbed inflow conditions. None of the measurements come with data on turbulence intensity and on turbulent length scale. The main design parameters of the compressor are summarized in Table 1. The total pressure inlet distortion is generated by a non-rotating wake generator with steel bars, upstream of the compressor stage. The circumferential extent of the investigated distortions is 120°.

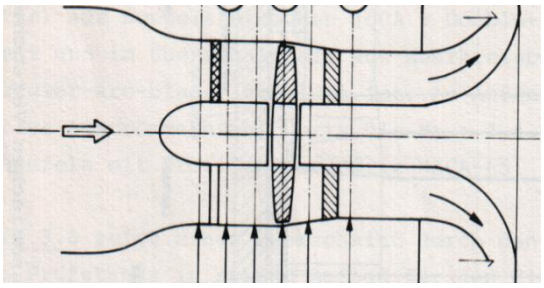

Figure 1: DLR Transonic Compressor Stage Test Rig [5]

2.2. TUD compressor stage

The second test case under consideration is the transonic compressor at the Technische Universität Darmstadt (TUD). A schematic sketch is shown in Figure 2. In this paper the Rotor-1/Stator-1 configuration is used. The rotor consists of 16 blades, and the stator of 29 vanes. The blades as well as the vanes have CDA (Controlled Diffusion Aerfoil) profiles. With its low aspect ratio and large tip clearance, the compressor stage features pronounced three-dimensional flows in the endwall regions. The general design parameters are listed in Table 1. More information about this compressor

configuration and the design objectives is provided in [8,9].

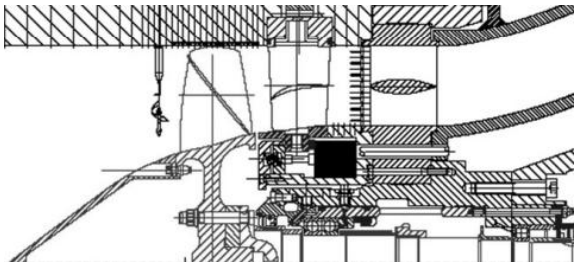

Figure 2: TUD Transonic Compressor Facility [9]

Table 1: Design Parameters at Design Point of the compressor stages

	DLR compressor	TUD compressor
Corrected Mass Flow Rate	17.3 $\frac{kg}{s}$	16 $\frac{kg}{s}$
Total Pressure Rate	1.5	1.5
Corrected Tip Speed at 100% shaft speed	424 $\frac{m}{s}$	398 $\frac{m}{s}$
Shaft Speed 100%	20260 rpm	20000 rpm
Tip Clearance gap	0.3 mm	1.6 mm
Number of Blades	28	16
Number of Vanes	72	29
Aspect Ratio	2	1.5

2.3. Numerical Method

2.4. Solver

All numerical investigations presented in this paper are carried out with the flow solver TRACE. The solver was developed by the DLR institute of propulsion technology (DLR-AT) in collaboration with MTU Aero Engines. It solves the unsteady Reynolds averaged Navier-Stokes equations using a finite volume approach. The solver is optimized for the computation of internal flows in turbomachines. All calculations presented in this study, are discretized second order accurate both spatial and temporal. Turbulent flow is taken into account by using the Wilcox [10] k-ω turbulence model. Transition phenomena are modeled with the γ-Re_θ model according to [11]. For more detailed information about TRACE refer to Kožulović et al.[12,13], Yang et al. [14,15], Nürnberger [16], Eulitz [17].

3 Simulation Setup and Grids

The simulations are carried out with structured grids, generated with the meshing tool G3DHEXA, which was also developed by DLR-AT. The grid has a typical OCH topology at the blades and vanes, and an H-topology at the passage, the inlet, and the outlet block of the blades and vanes. A special H-block meshes the tip clearance. 91 blade-to-blade, 57 spanwise, and 130 axial grid points resolve one passage of the DLR-rotor. The small tip clearance of the DLR-rotor is discretized by 7 grid points. The stator vane consists of 85, 57, 110 grid points for blade-to-blade, spanwise, and axial direction, respectively. This leads to a total number of 50 million cells for the whole full annulus DLR compressor, including the inlet and outlet blocks.

Due to different blade and vane pitch, the grid points vary slightly for the TUD compressor. The TUD rotor is discretized by 111, 80 and 147 and the TUD stator by 97, 80 and 147 grid-points, for blade-to-blade, spanwise, and axial direction, respectively. 15 cells are necessary for the larger tip-clearance gap. The whole 360° TUD compressor domain contains about 56 million cells. In a common turbomachinery approach, wall boundary layer wall functions are used for the hub and tip and low Reynolds treatment for the blade and vane surfaces.

The steady inflow distortion is modeled by a non-reflecting Riemann boundary condition, modified to read in the inlet flow field. The inflow measurements from the experiments in [5] serve as inlet boundary condition for the DLR test case. Since the TUD compressor was never tested with inlet distortions similar to the DLR case a generic inlet distortion was used for the purpose of this study. The TUD test case involves a 60° pure total pressure distortion, in contrast to the DLR test case, with a combined 120° total pressure and inflow angle variation. The reason for choosing a pure total pressure distortion lies in the opportunity that it allows to investigate its effect more distinctly. The smaller distorted sector should reveal the effect of preferably small distortions on the efficiency. According to Cousins [18] a noticeable influence on the compressor performance is

expected for distorted sectors exceeding a critical angle which is calculated to an angle of about 15° for the TUD test case. Therefore a 60° sector is assumed to have a distinct influence. To guarantee comparability, the same grid resolution is used for the two-dimensional blade-to-blade calculations and for the 3D computations within this paper.

4 Global validation of the 3D Calculations

In order to demonstrate the ability of the 3D calculations to correctly predict the global flow field for uniform inflow conditions the numerical data was validated by experimental data. In Figure 3 it is shown the measured and numerically predicted speedline at 85% rotor speed for the DLR test case. A rotor speed of 85% has been chosen since most experimental data is available for this rotor speed. The speedlines are normalized to the operating point of peak efficiency in order to be able to compare the trends of experimental and numerical data better. The global trend of characteristics both for total pressure ratio and for the isentropic efficiency are in very good agreement. The differences between experimental and numerical data are 1%, both for isentropic efficiency and total pressure ratio at peak efficiency without normalization. The same good agreement of numerical and experimental results features the TUD test case shown in Figure 4.

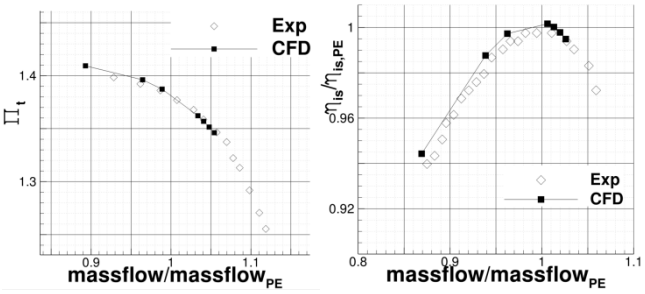

Figure 3: DLR test case; measured and numerically predicted speedline at 85% rotor speed

Hence, the three dimensional, numerical calculations are able to capture the general flow behavior for both test cases, very well for homogenous inflow conditions.

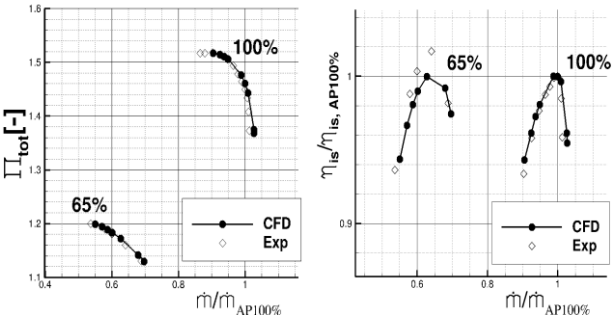

Figure 4: TUD test case; measured and numerically predicted speedlines for 65% and 100% rotor speed

5 Comparison between blade-to-blade and full 3D calculations

After validating the 3D calculations successfully with experimental data the results of 2D blade-to-blade calculations are validated with those of the 3D calculations.

5.1. Results for uniform inflow conditions

DLR test case

Given that the unsteadiness of the flow-field is negligible in homogeneous inflow conditions, the calculations with uniform inflow conditions are performed with steady-state flow. The interface between rotor and stator is modeled by a mixing plane approach, a common approach for flow simulations in turbomachinery. In Figure 6 and Figure 5, the relative Mach number distribution at 50% blade height is shown for the 2D and 3D simulation, respectively. The flow-field corresponds to the peak efficiency operation point. For the 3D calculation, the relative inlet Mach number is about 0.86 and the meridional flow angle is about 65° with respect to the axial direction. At 50% blade height, the flow-field and passage flow show the typical behavior for high subsonic inflow. On the suction surface the accelerating fluid forms a supersonic area at the front part of the blade, which ends with a normal shock at 8% axial chord. The fluid decelerates in the diffusing part of the blade passage. The 2D blade-to-blade calculations in Figure 6 show the shock position slightly shifted further downstream compared to

the 3D results. Whereas the rotor wake and the stator flow show a very similar behavior. In general the form of the supersonic area, the shock position, and the behavior in the diffusing part of the blade cannel are reasonable and coincide in 2D and 3D calculations.

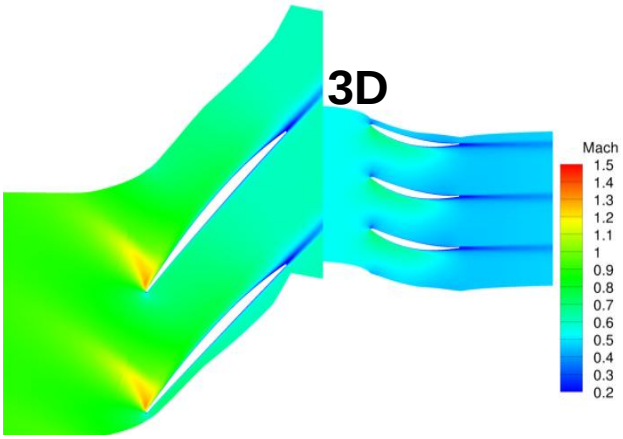

Figure 5: Relative Mach number distribution at 50% blade height, 3D calculation, DLR test case

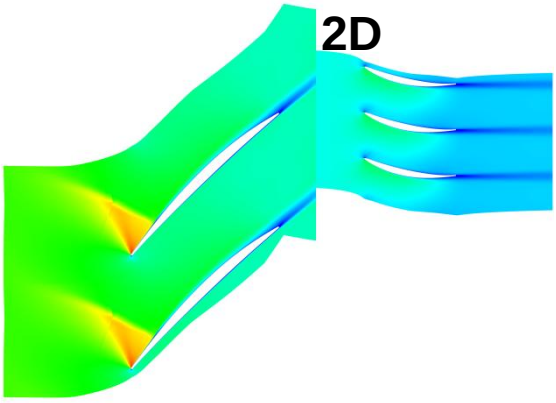

Figure 6: Relative Mach number distribution at 50% blade height, 2D calculation, DLR test case (levels see Figure 5)

TUD test case

2D blade-to-blade calculations are also validated for the TUD test case with uniform inflow conditions. The TUD test case under uniform inflow conditions has already been investigated with the help of 3D calculations, published in [19]. Figure 7 and Figure 8 show the flow-field of this test case obtained by 3D and 2D flow simulations, respectively.

The general flow field differs significantly between 2D and 3D calculations, in particular within the rotor passage.

Due to the different relative Mach number distribution for the same back pressure, it was initially assumed that the strong 3D flow in this test case leads to a different operating conditions in the 3D and 2D simulations. An increase of the back pressure leads to a strong flow separation at the stator vane suction side vane, which is not reproduced by the 3D data.

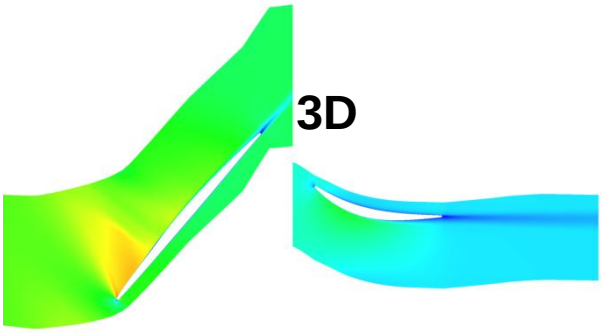

Figure 7: TUD test case, uniform inflow relative Mach number 3D, (levels see Figure 5)

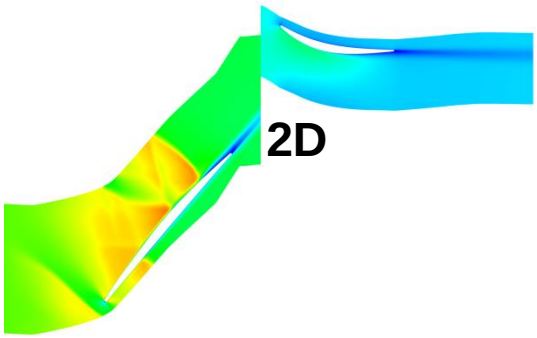

Figure 8: TUD test case, uniform inflow, relative Mach number distribution, 2D blade-to-blade (levels see Figure 5)

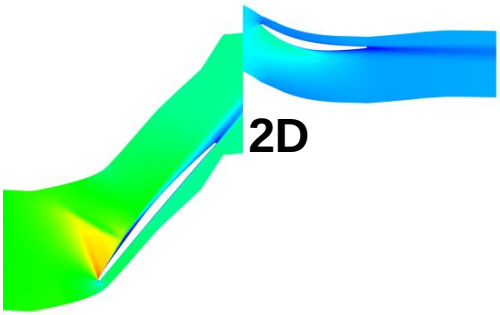

Figure 9: TUD test case, relative Mach number 2D blade-to-blade with 90% rotor speed

Still, a variation of the rotor speed of 10% leads to a flow-field, which is more similar to the blade-to-blade flow-field of the 3D calculations. Figure 9 shows the relative Mach number distribution for 2D calculations with 90% rotor speed. The inflow is subsonic, the supersonic area is limited to the front part of the blade and the level of relative Mach number is almost the same in the 3D as well as in the 2D simulation.

It goes without saying that the flow fields are still slightly varying. Nevertheless, it is assumed that the similarity is good enough to study the global trend of the compressor´s response with 2D blade-to-blade calculations.

5.2. Results for non-uniform inflow conditions

DLR test case

In Figure 10 the inlet boundary conditions of the DLR test case are shown. The inflow distortion consists of a total pressure and an inflow angle variation. The total pressure loss, and therefore the lower axial velocity, can be supposed to result in higher leading edge incidences. Whereas, the inflow angle variation exhibits a decrease in incidence angle initially, until increasing in the distorted sector.

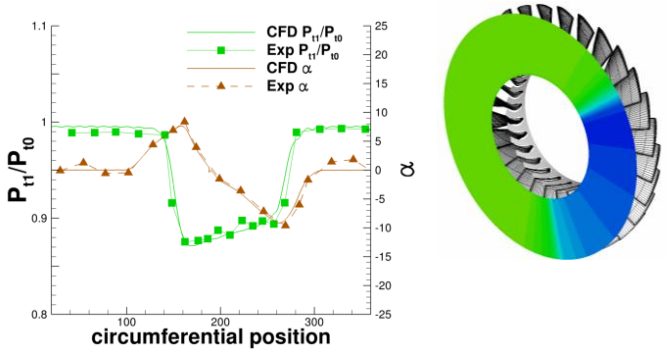

Figure 10: Prescribed P_t and flow angle (α) Variation (left), P_t distribution at inlet boundary, DLR test case (right)

Figure 11 depicts the circumferential total pressure ratio in the interface plane between rotor and stator at mid-span. Numerical 2D, 3D, and experimental data are compared to each other. The rotor enters the distorted sector at about 120°. However, the total pressure ratio is already influenced prior to this. After a fast decline to the minimum, the total pressure ratio rises again to the undistorted level at about 280°. The gradient of the decrease of the total pressure ratio at the rotor blade's entry of the distorted sector is higher than the gradient of the increase within and at the blade's exit of the distortion sector. This behavior results from the combination of the inflow angle and the total pressure distortion. Entering the distorted sector, the inflow angle variation causes a negative incidence that leads to a lower total pressure ratio. Furthermore, the inflow total pressure decreases, too. Both effects combined lead to a steep decline. However, the inflow angle attains its maximum at the beginning of the distorted sector and decreases in the following to reach its minimum at 280°. This leads to a higher incidence as well as to a steeper increase of the total pressure ratio. The total pressure distortion within the distorted sector is not constant either, but increases slightly. The total pressure and inflow angle variation lead to a smoother increase of the total pressure ratio within and at the exit of the distorted sector.

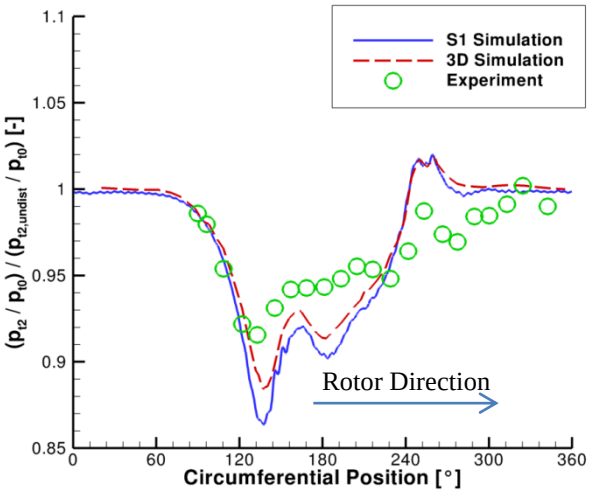

Figure 11: DLR test case, normalized total pressure ratio between rotor and stator

The results of the 2D S1 blade-to-blade and 3D simulations show a very good agreement as depicted in Figure 11. Both trends coincide, for the rotor entering the distorted sector as well as for its behavior within the sector and for its exit out of the critical sector. There are only few minor differences between the 3D and the 2D calculations. The minimum of the total pressure ratio for example, is lower in the 2D than in 3D calculation. In contrast to that, the numerical and experimental differences differ much more. General trends are reproduced very well however, there are some quantitative differences. This is of no major concern since the focus of this study lies on the difference between 2D and 3D calculations. A more thorough validation of the 3D data and the experimental results can be found in [20,21].
The total temperature rise is shown in Figure 12. The global behavior of the total temperature and

of the energy addition from the rotor to the fluid can be attributed to the variation of the incidence as already discussed for total pressure. Decreasing incidence in the first part of the distorted sector and increasing incidence in the second part lead to lower circumferential total temperature and higher total temperature after the rotor. The numerical data coincides very well, as it does for the total pressure ratio. The trends of the experimental and numerical data also agree well, with only minor deviations. Therefore, it can be concluded that the results of the 2D and 3D calculations for the DLR test case coincide both qualitatively and quantitatively.

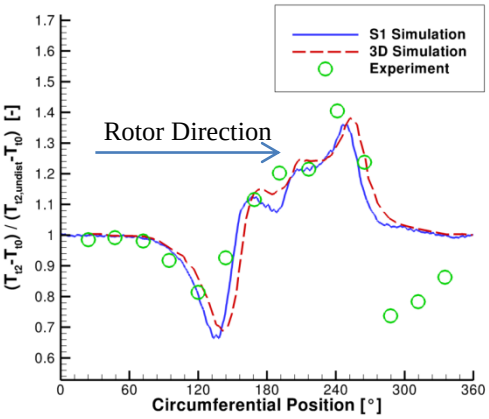

Figure 12: DLR test case, total temperature rise between rotor and stator

DLR test case: Mid-span relative Mach number

For a deeper examination of the blade-to-blade flow with non-uniform inflow in Figure 13 the relative Mach number distribution at 50% blade height is shown. The left hand side depicts the 3D data and the right hand side the results from the 2D bade-to-blade simulation. As can be seen the inflow distortion influences both the rotor and the stator flow. The shock position, the shape of the supersonic area, and the blade and vane wakes vary strongly during the phase the blade moves through the distorted sector. At the entry of the distorted sector the blade flow is almost purely subsonic, only close to the leading edge the flow accelerates to supersonic Mach numbers (A). The stator vane wakes are very pronounced at the same circumferential position (B). Within the distorted sector (A to C) the shock position moves downstream and the maximum Mach numbers reached in the supersonic area are rising. The wakes of the vane flow getting less pronounced.

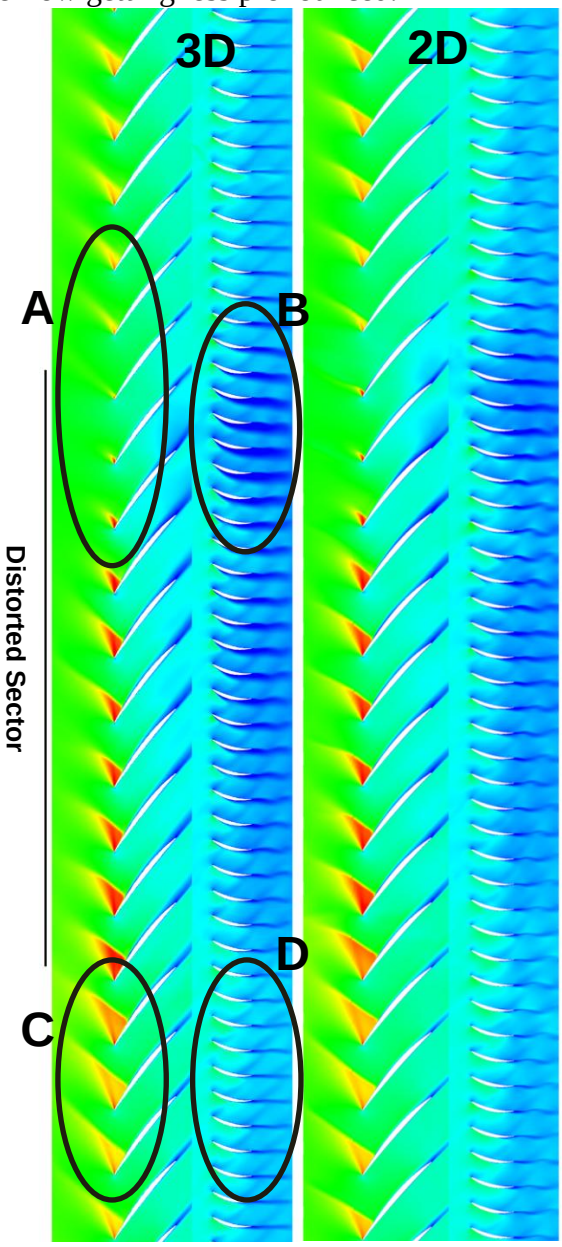

Figure 13: DLR Test Case, Relative Mach Number at Mid-Span with non-uniform Inflow Conditions 3D (left) and 2D (right)

When reaching the exit of the distorted sector the shock position is most downstream and the supersonic area is biggest, but the level of the reached Mach numbers is significantly lower (C). In addition, the vane flow field shows slightly higher Mach numbers after the distorted sector (D) until to reach the level of the undistorted flow field after about three vane passages.

In order to a better understanding of the occurring flow phenomena the inlet static and total pressure distributions at 50% blade height are depicted in Figure 14. The periodic variation of the static pressure distribution is due to the potential fields of the rotor blades. The variation of static pressure is part of the compressor's response to inhomogeneous inflow as discussed in [1,22].

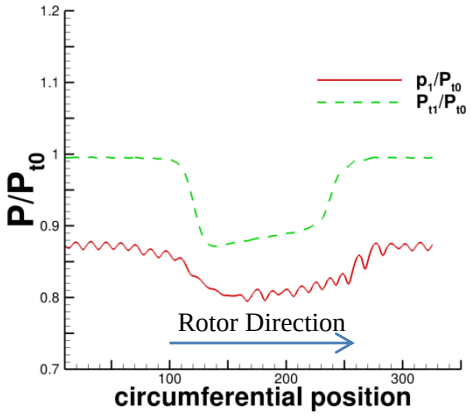

Figure 14: DLR test case, Static and total inlet pressure

At the distortion entry the total pressure and hence the axial velocity declines, which result in the upstream movement of the shock position and a smaller supersonic area. The lower axial velocity leads to a higher vane incidence causing flow separation on the vane which results in pronounced vane wakes. This flow separation (A, cf. Figure 13) is also observed in the eddy viscosity distribution, which is not shown here. During the blade's travel through the distorted sector the total pressure, the axial velocity, and the blade incidence are increasing. This increase causes the shock to move downstream and the supersonic area to increase. In contrast, the vane incidence is decreasing as a result from the increasing total pressure (cf. Figure 11) and the increasing axial velocity. This decrease causes a less pronounced vane flow wake.

After the blade exits the distorted sector, the static pressure recovers later than the total pressure to the level of the undistorted sector which results in the maximum axial velocity. The high axial velocity in combination with low incidence leads to the shocks most downstream position, but with moderate Mach number level in the supersonic area. Also, the vane flow shows the highest Mach numbers in this region.

From the variation of the rotor blade flow it can be concluded that the inflow distortion causes also a variation of blade loading. Varying mechanical stresses which result can endanger the mechanical integrity of the blade and the operational safety of the compressor. The variation of the aerodynamic blade loads during the blade's travel through the distorted sector is shown in Figure 15. In this, case a loading parameter is used which relates the averaged pressure difference between suction and pressure side in the distorted sector to the respective value of the undistorted case.

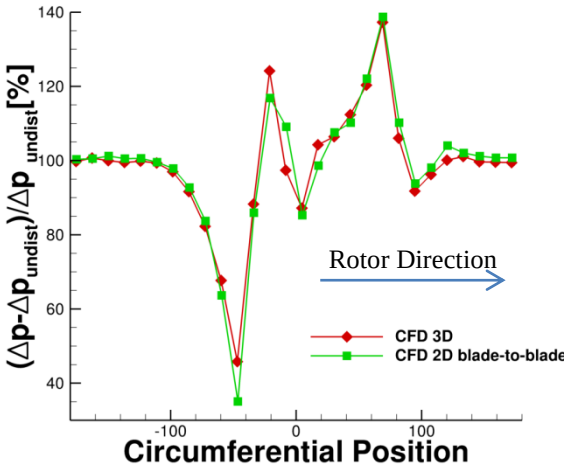

Figure 15: DLR test case, circumferential blade loading parameter

The loading parameter follows the total energy rise variation in Figure 12. The total temperature rise depicts the transfer of energy from the rotor to the fluid and is, therefore, related to the blade loading. The blade loads show a very strong variation. The blade experiences a minimum of 40% and a maximum of 140% of undistorted blade load within the distorted sector. That means the excitation amplitude is as high as the mean load and the excitation frequency is three times the rotational frequency since the distorted sector covers 120°. As can be seen, the 2D and 3D calculations are in very good agreement. In this test case, a 2D calculation predicts the flow behavior at mid span almost as well as a full 3D calculation for the peak efficiency operating point.

The inflow distortion in the DLR test case shows a strong interaction between total

pressure distortion and inflow angle distortion. In order to study the influence of a total pressure distortion a generic pure total pressure distortion pattern was used for the study of the TUD test case outlined in the following.

TUD test case

The generic 60° sector pure total pressure distortion is used in the TUD test case as shown in Figure 16. It is shaped as a step function in order to minimize the influence of the inflow angle variation and to generate a symmetric distortion pattern. A symmetric shape is used in order to study if the rotor response is different at the entry and at the exit of the distorted sector. Figure 17 shows the variation of the total pressure ratio after the rotor. Upstream of a compressor, operating with non-uniform inflow, flow redistribution takes place that leads to a variation of the inlet static pressure [1,22]. The static pressure gradients deflect the inlet flowfield vector resulting in an inflow angle variation. Therefore, a moderate inflow angle variation at the rotor leading edges is expected although with a symmetric pure total pressure distortion pattern.

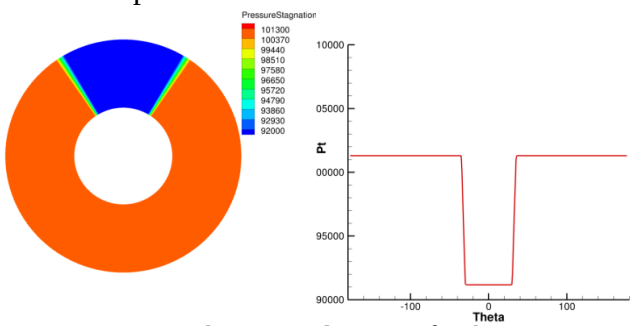

Figure 16: Total pressure distortion for the TUD test case

For the 3D calculations, the normalized total pressure ratio decreases as soon as the blade enters the distorted sector, and increases at the end of the distorted sector. Both the initial decline and the subsequent increase are quite steep. This behavior is to be expected due to the particular shape and the symmetry of the distortion. However, the variation of the normalized total pressure ratio is not absolutely symmetric: at the exit of the distorted sector, the total pressure ratio slightly exceeds the level from the undistorted sector as shown in Figure 17. The same trend can be observed for the total temperature rise shown in Figure 18.

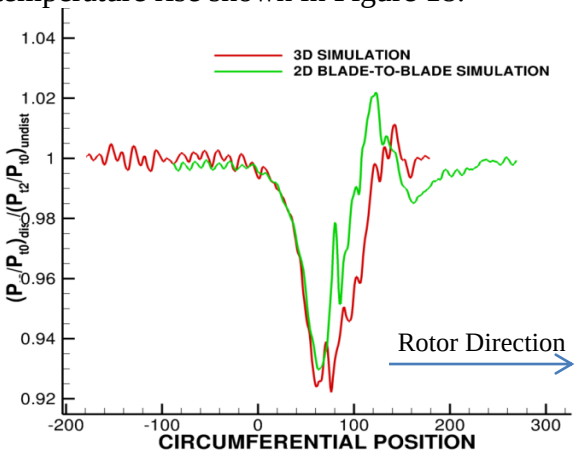

Figure 17: TUD test case, circumferential total pressure ratio between rotor and stator

The total temperature rise decreases initially, before ascending due to the incidence variation, which in turn can be attributed to the total pressure distortion. The variation of the inflow angle, discussed above, is considered responsible for the non-symmetric behavior of the total pressure ratio and of the total temperature rise. The initial drop of the total temperature can be attributed to an incidence variation, as discussed for the DLR test case above.

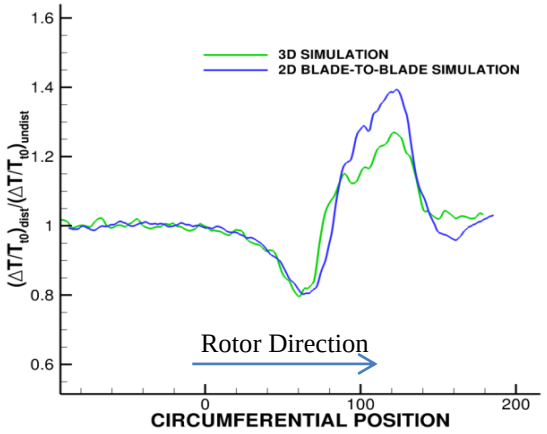

Figure 18: TUD test case, circumferential total temperature rise between stator and rotor

Both the 2D and the 3D calculations predict the general trends quite similarly. The circumferential variation of the total pressure ratio, the sharp decline at the beginning and the steep rise at the end of the distorted sector, are equally displayed, by both the 2D and the 3D calculation. The extension of the distortion influence zone is smaller in the 2D calculations,

and the maximum of the total pressure ratio is overestimated. The total temperature rise in Figure 18 shows the same behavior: the trend is predicted similarly. The maximum, however, is predicted too high, and the 2D simulation depicts a drop of the total temperature at the exit of the distorted area, which is not present in the 3D calculations.

TUD test case: Mid-span relative Mach number

Figure 19 shows the relative Mach number distribution at 50% blade height for the TUD test case. On the right hand side again 3D data are shown and on the left hand side 2D data. Similar flow phenomena like for the DLR test case dominate the flow field. The variation of the supersonic area and the shock position are similar. At the entry the supersonic area decreases, increases within the distorted sector until reaching its major extent after the blade exits the distorted sector. However, in comparison to the DLR test case there are some differences due to the pure total pressure distortion and the smaller extent of the distortion. These differences in the rotor flow were already discussed above. The stator flow shows lower Mach numbers and pronounced wakes within the distorted sector. The shape of the vane wakes, however, remains almost constant within the distorted sector in contrast to the DLR test case. The generic distortion pattern is symmetric for the TUD test case, which results in almost less variation of the stator flow field compared to the DLR test case.

The 3D and 2D data are in good qualitative agreement. However, there are some quantitative differences in the undistorted sector as well as in the distorted sector. The relative Mach number is slightly higher in the stator row for the 2D blade-to-blade calculation.

Figure 20 shows the results for the variation of blade loading. The maximum of 120% and the minimum of 80% mean load are lower in comparison to the DLR test case. The reason for the lower extrema is the lower inflow angle variation in the TUD test case. In the DLR test case this causes an additional blade loading variation. The excitation amplitude is about 40% of the mean blade load in the 3D data. The 2D blade-to-blade calculation predicts the trend similar, but overestimates minimum and maximum, which results in an excitation amplitude of almost 70% blade load.

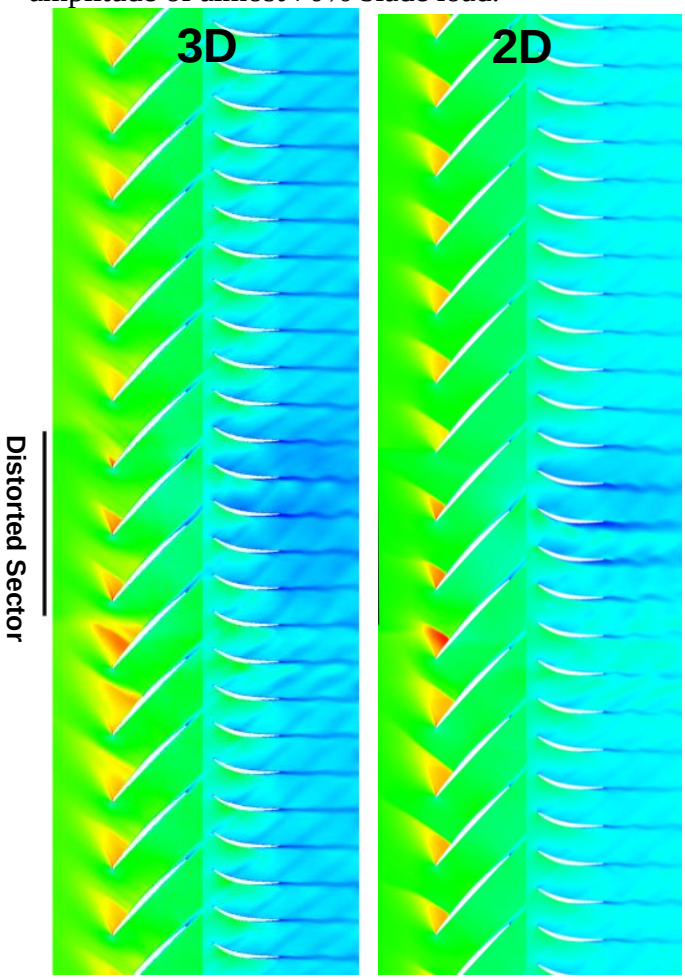

Figure 19: THD Test Case, Relative Mach Number at Mid-Span with non-uniform Inflow 3D (left) and 2D (right)

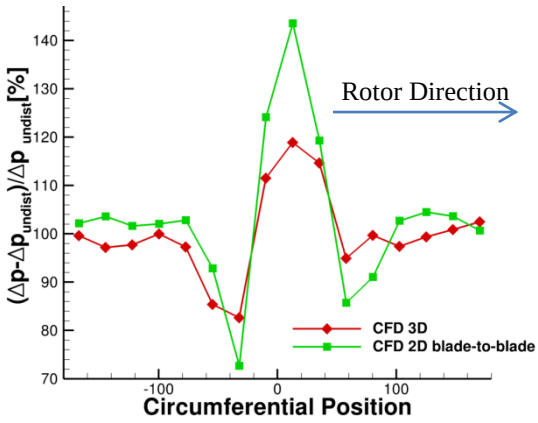

Figure 20: TUD Test Case, Circumferential Pressure Difference between Suction and Pressure Side

To sum up, the 2D blade-to-blade calculation of the TUD test case is only able to predict the global trend of the compressor's response to distorted inflow conditions. The TUD test case design features pronounced stronger three-dimensional flows, which limit the prediction capability of 2D blade-to-blade simulations.

6 Conclusions

This study numerically investigates two transonic axial compressor stages for the peak efficiency operating point under uniform as well as under non-uniform inflow conditions. The compressor stages under investigation have very similar global parameters, but different design philosophies. The DLR test case design results in a minor secondary flow field, whereas the TUD test case design features pronounced 3D flows. The investigation involves two modes of compressor simulation: a full-annulus 3D and a full-annulus 2D blade-to-blade simulation at mid-span. The compressor's response to non-uniform inflow is investigated with the help of the full-annulus 3D simulations. Furthermore, the capability of two dimensional blade-to-blade calculations is tested by validating the 2D results with the full 3D data.

Initially, the results of the 3D calculations for uniform inflow are validated successfully with experimental data for the two test cases. The 2D blade-to-blade results of the DLR test case are in good agreement to the full 3D simulation. This contrasts with the TUD test case, where reasonable results for uniform inflow are only obtained at 10% less rotor speed.

For non-uniform inflow, the 3D results show that both the inflow angle and the total pressure variation have an impact on the extent to which the flow behavior depends on the inlet distortion. In particular, the combination of inflow angle and axial velocity variation in the DLR test case results in an enhancement of the total pressure deficit and the total temperature rise. This enhancement results in a severe variation of blade loading and mechanical excitation, additionally. Furthermore, the stator flow and flow separation within the stator passages also triggered by the inflow angle and axial velocity, have an important influence on the compressor stage performance .

The TUD test case shows similar results, but with a lower variation of total temperature and blade loading due to the absence of an inflow angle variation. Similarly to the results under non-uniform inflow conditions, the blade-to-blade calculations show better results for the DLR test case than for the TUD test case.

For the DLR test case, the blade-to-blade calculation predicts the flow field at mid-span almost as accurately as the 3D calculation. On the other hand, the results of the TUD test case under non-uniform inflow conditions show stronger deviations between 2D and 3D. The blade-to-blade calculation can predict the trend quite well, although it exhibits significant quantitative deviations.

In a nutshell, this study allows for the conclusion that blade-to-blade calculations work well for compressors with a weak secondary flow field, both under uniform and under non-uniform inflow conditions. The reliability of the 2D blade-to-blade calculation decreases with an increase of the 3D flow character. In general terms it is possible to adequately predict and to assess for both test cases how a total pressure inflow distortion will qualitatively influence the flow behavior.

Acknowledgments

The authors gratefully acknowledge the support of the "Deutsche Forschungsgemeinschaft DFG" (German Research Foundation) which funded this research project.

References

[1] Longley J. P., and Greitzer E. M., 1992, "Inlet Distortion Effects in Aircraft Propulsion System Integration," AGARD-LS-183.

[2] Gunn E. J., Tooze S. E., Hall C. A., and Colin Y., 2012, "An Experimental Study of Loss Sources in a Fan Operating with Continuous Inlet Stagnation Pressure Distortion," GT2012-68888.

[3] Yao J., Gorrell S. E., and Wadia A. R., 2010, "High-Fidelity Numerical Analysis of Per-Rev-Type Inlet Distortion Transfer in Multistage Fans-Part I: Simulations With Selected Blade Rows," Journal of Turbomachinery, **132**(041014), pp. 1-10.

[4] Yao J., Gorrell S. E., and Wadia A. R., 2010, "High-Fidelity Numerical Analysis of Per-Rev-Type Inlet Distortion Transfer in Multistage Fans—Part II: Entire Component Simulation and Investigation," Journal of Turbomachinery, **132**(041015), pp. 1-17.

[5] Lecht M., 1983, "Beitrag zum Verhalten von Axialverdichterstufen," "RWTH Aachen," PhD thesis.

[6] Dunker R. J., and Hungenberg H., 1980, "Transonic axial compressor using laser anemometry and unsteady measurements," AIAA Journal, **18**.

[7] Dunker R., Strinning P., and Weyer H., 1978, "Experimental study of the flow field within a transonic axial compressor rotor by laser velocimetry and comparison with through-flow calculations.," Journal of Eng. for Power, **100**(2), pp. 279-287.

[8] Schulze G., 1996, "Betriebsverhalten eines transsonischen Axialverdichters," "TH Darmstadt," PhD thesis.

[9] Bergner J., and Hennecke D. K., 2004, "Entwicklung von Verdichterrotoren für einen einstufigen, transsonischen Axialverdichter-prüfstand," Deutscher Luft- und Raumfahrt-kongress, Dresden.

[10] Wilcox D., 1998, Turbulence modeling for CFD., DCW Industries, Anaheim.

[11] Menter F. R., Langtry R. B., Likki S. R., Suzen Y. B., Huang P. G., and Völker S., 2008, "A Correlation-Based Transition Model Using Local Variables— Part I: Model Formulation," Journal of Turbomachinery, **128** (3), pp. 413-422.

[12] Kožulović D., 2007, "Modellierung des Grenzschichtumschlags bei Turbomaschinen-strömungen unter Berücksichtigung mehrerer Umschlagsarten.," "Ruhr-Universität Bochum."

[13] Kožulović D., Röber T., Kügeler E., and Nürnberger D., 2004, "Modifications of a two-equation turbulence model for turbomachinery fluid flows.," Deutscher Luft- und Raumfahrtkongress, Dresden.

[14] Yang H., Nürnberger D., and Kersken H.-P., 2006, "Toward excellence in turbomachinery computational fluid dynamics: A hybrid structured-unstructured reynolds-averaged navier-stokes solver.," Journal of Turbomachinery, **128**, pp. 390–402.

[15] Yang H., Nürnberger D., and Weber A., 2002, "A conservative zonal approach with applications to unsteady turbomachinery flows.," DGLR-JT2002-073.

[16] Nürnberger D., 2004, "Implizite Zeitintegration für die Simulation von Turbomaschinenströmungen.," DLR Forschungsbericht 2004-27.

[17] Eulitz F., 2000, "Numerische Simulation und Modellierung der instationären Strömung in Turbomaschinenkomponenten.," "Ruhr-Universität Bochum, Germany," PhD thesis.

[18] Cousins W. T., 2004, "History, Philosophy, Physics, and Future Directions of Aircraft Propulsion System / Inlet Integration," GT2004-54210.

[19] Ciorciari R., Lesser A., Blaim F., and Niehuis R., 2012, "Numerical Investigation of Tip Clearance Effects in an Axial Transonic Compressor.," Journal of Thermal Science, **21**(1).

[20] Lesser A., and Niehuis R., 2011, "Detailed Numerical Investigation of a Transonic Axial Compressor Stage with Inlet Distortions," ISAIF10-106.

[21] Lesser A., Iseler J., and Niehuis R., 2011, "Numerical Investigation of a Highly Loaded Axial Compressor Stage with Inlet Distortions," GT2011-46457.

[22] Mazzawy R. S., 1977, "Multiple Segment Parallel compressor Model for Circumferential Flow Distortion," Journal of Engineering for Power, **99**(2), pp. 288-297.

Copyright Statement